How Topographic Slopes Control Gravity-spreading in Salt-bearing Passive Margins

Zhiyuan Ge[1,2,3], Matthias Rosenau[4] and Michael Warsitzka[5]

[1] State Key Laboratory of Petroleum Resources and Prospecting, China University of Petroleum (Beijing), Beijing, 102249, China.

[2] College of Geosciences, China University of Petroleum (Beijing), Beijing, 102249, China.

[3] Department of Earth Science, University of Bergen, Allégaten 41, 5007 Bergen, Norway.

[4] Helmholtz Centre Potsdam – GFZ German Research Centre for Geosciences, 14473 Potsdam, Germany.

[5] Institute of Geophysics of the Czech Academy of Sciences, Boční II/1401, 141 31 Prague 4, Czech Republic.

Corresponding author: Zhiyuan Ge (gezhiyuan@cup.edu.cn)

Key Points:

- We highlight how geometric variations within the sediment wedge can control gravity-spreading in salt-bearing passive margins.
- We test two wedges constrained by sedimentary systems and critical taper theory and demonstrate their influences on viscous salt flow.
- The two wedge geometries represent two endmembers with diagnostic structural and kinematic characteristics that can be identified in nature.

Abstract

Sediment spreading is a key process during gravity-driven deformation in salt-bearing passive margins. Whether and how progradational sedimentary wedges control gravity-spreading is still under debate. We use analogue modelling to compare two endmember configurations constrained by critical wedge theory, where the initial depositional slopes are: a 5°critical (stable) slope and a 27° unstable slope. In both configurations, differential loading initiates spreading characterized by a basinward migrating system of proximal extension and distal contraction. With a critical frontal slope, the translational domain expands as the contractional domain migrates forward with viscous flow evenly distributed. With a steep frontal slope, both extensional and contractional domains migrate due to more localized viscous flow under the wedge toe producing diagnostic structures of late extension overprinting early contraction. In both cases, salt flow is dominated by Poiseuille flow. Our study highlights that geometric variations of sedimentary wedges result in variable responses in gravity-spreading systems.

Plain Language Summary

In areas such as Gulf of Mexico, the seafloor topography is largely controlled by subsurface salt-related deformation, which is in turn important for habitat and ecosystem studies as well as sedimentary systems within. Studies have debated whether such deformation can be driven purely by sediment deposition. We use laboratory models consisting of sand and silicone to study the influence of sediment loading on salt-involved deformation. We find that the frontal slope gradient of the sediment wedge has significant influences on the deformation. Therefore, the depositional system itself becomes critically important for understanding the evolution of the seafloor topography.

1 Introduction

Gravity-driven tectonic deformation has been widely observed in salt-bearing passive margins (e.g. Brun & Fort, 2011; Rowan et al., 2004) (Fig. 1a). As the sediment progrades and deforms under its own weight above a basal evaporite layer, a typical linked system occurs with a zone of proximal extension and a corresponding zone of distal contraction (e.g. Fort et al., 2004; Rowan et al., 2004). Two basic modes have been proposed to describe such gravity-driven deformation: 1. gravity-gliding controlled by the basal slope of the detachment layer; 2. gravity-spreading associated with the collapse of a progradational sediment wedge due to differential loading (e.g. Brun & Fort, 2011; Raillard et al., 1997; Rowan et al., 2004). However, whether or how gravity spreading dynamics can influence or even dominate a gravity-driven salt tectonic system is a matter of controversial debate (e.g. Brun & Fort, 2011; Rowan et al., 2012).

One of the problems prohibiting our understanding of gravity spreading is that sediment progradation is often oversimplified in modelling studies focusing on salt tectonics. Sediment progradation is generally simulated as a wedge-shaped sediment cover (e.g. Cohen & Hardy, 1996; Ge et al., 1997; Krézsek et al., 2007; McClay et al., 1998), with loosely defined sedimentological meanings. For example, the progradational rate and thickness of a sedimentary wedge are based on the interpolation of overall sediment cover thickness from a few sites in the basin (e.g. Adam et al., 2012; McClay et al., 1998). Even when specified with some sedimentological implications, the geometric variations of the progradational wedges are rarely explored (e.g. Ge et al., 1997; Gemmer et al., 2005; Gradmann et al., 2009).

In this study, using analogue modelling, we investigate the structural and kinematic evolution of a passive margin salt tectonic system driven solely by progradation of sedimentary wedges. We use sedimentological constrains and critical taper theory to select two wedge geometries, one with a critically stable and the other with an extensionally unstable frontal slope. Our models demonstrate how geometric variation of the progradational wedge alone is able to control the dynamics of a thin-skinned gravity-spreading system. These results thus resolve some controversies of salt tectonics in passive margins and provides additional application of critical taper theory and salt flow analysis to salt tectonics in general.

2 Materials and Methods

2.1 Geometry of sedimentary wedges

Progradational systems have been modelled as a sedimentary wedge thinning from proximal to distal (e.g. Brun & Fort, 2011; Ge et al., 1997; Gemmer et al., 2005; Gradmann et al., 2009; McClay et al., 1998; Vendeville, 2005). At natural scales, the sedimentary wedges in such models typically have thicknesses of a few 100s to 1000s of metres (e.g. Adam & Krezsek, 2012; Patruno & Helland-Hansen, 2018), and are consistent with typical natural depositional slopes of <5° (e.g. Carvajal et al., 2009; Prather et al., 2017). However, in some cases, depositional slopes can be much steeper and close to the local angle of repose. For instance, sea level changes, tectonics, and carbonate deposition can cause local slopes up to 30° (e.g. Prather et al., 2017; Ross et al., 1994; Schlager & Camber, 1986). In the North Gulf of Mexico, for instance, some of the seafloor profiles crossing the salt-related structures show slopes up to 20° (Lugo-Fernández & Morin, 2004; Roberts et al., 1999). At a smaller scale, Gilbert-type deltas usually have subaqueous slopes between 20–27° (Nemec, 1990).

2.2 Constraints from Critical Wedge theory (CWT)

We hypothesize that a geometric variation in the frontal slope impose an important boundary condition and has an effect on the force balance and thus the spreading dynamics of progradational wedges similar to accretionary wedges often analysed in the framework of the critical coulomb wedge (or taper) theory (e.g. Dahlen, 1990). According to CWT, a stability criterion can be defined for a brittle wedge, which is a function of its surface and basal slopes (α and β respectively), the (effective) basal and internal strength as well as the densities of the solid and pore fluid phases (e.g. Dahlen, 1990). Plotting the stability criterion into a α vs. β diagram results in a stability field or failure envelope, which represents the critical state geometry (Figs 1b, S1 and Text S1). Geometries (tapers) plotting above the envelope are extensionally unstable while geometries below are contractionally unstable. Both wedges tend to deform until the critical geometry in force balance is reached. From a static point of view, any wedge slope above a viscous layer tends to relax to a very low taper (<1°) due to the low long term strength of the underlying viscous layer (Davis & Engelder, 1985). In a dynamic system, such as realized in the presented study, the deformation is continuously driven by sediment progradation. Hence, the geometric evolution is disturbed continuously. Applying CWT suggests that gentle slopes of sedimentary wedge (~5°) are just at or slightly beyond the verge of failure (i.e. the critical state) whereas steep slopes (20–30°) are deeply in the extensionally unstable regime (Fig. 1b). Since the distance to the stability envelope is proportional to the force imbalance, we hypothesize that the two scenarios represent endmembers of close to stable (or critical) and highly unstable wedges, the spreading dynamics of which should vary dramatically.

2.3 Experimental setup

To test the effect of wedge stability on spreading dynamics, we use an analogue modelling approach that simulates complex salt tectonic evolution similar to previous studies (e.g. Brun & Fort, 2011; Ge et al., 2019a; Ge et al., 2019b; McClay et al., 1998; Vendeville, 2005). The general approach and materials used are described in detail by Ge et al. (2019a). We use a geometric scaling ratio of 10^{-5} (i.e. 1 cm in the model ≈ 1 km in nature) and a time scaling ratio of ~10^{-10} (i.e. 4 hours in the model ≈ 1 Ma in nature) based on standard scaling procedures (e.g. Adam & Krezsek, 2012) (Table S1). A basal sand body on top of a rigid basal plate forms the mould of two identical silicone basins (Fig. 1c). After sieving a pre-kinematic granular layer over the silicone layer, the simulation starts with the emplacement of two sand wedges.

Compared to a setup with an even thickness silicone, the double-wedge shape of the silicone base is a more realistic representation of a passive margin salt basins (Brun & Fort, 2011). We note that the variation in silicone thickness may lead to spatial strength variations within the viscous silicone. However, stability analysis shows that a spatial (or temporal) variation of even one order of magnitude in basal strength has little impact upon the stability fields (Fig. 1b).

We test two syn-kinematic sedimentary wedges. Initially, the first mode has a critical slope (5°, Model 1) and the second model has a steep, unstable slope (27°, Model 2). Both wedges prograde basinward at the same rate of 10 cm day^{-1} (~10 km in 6 Ma) with an aggradational rate of 2 mm day^{-1} (~200 m in 6 Ma) (Fig. 1c), falling into the slower end of natural progradational systems (e.g. Carvajal et al., 2009). The frontal slope decreases to 2.6° in Model 1 and increases to 34.2° in Model 2 towards the end of the experiment (Fig. 1c). Thus, the stability analysis is still valid for both wedges during the experiment, although the actual frontal slope may vary slightly due to sieving more sand in topographically low areas (Fig. 1b). The different geometries of the two wedges reflect the variable amounts of sediment input (Fig. 1c). Both models start with a 25 mm thick cover onto which a maximum of 4 mm (Model 1) and 25 mm (Model 2) are added by sieving every 12 hours over a duration of 5 days (Fig. 2a). For simplicity, no lateral variations of sedimentation are considered.

During the experiment, we monitor the model surface with a stereoscopic pair of cameras and apply digital image correlation (LaVision Davis 8, see details in Ge et al., 2020). The result is the 3D topography and incremental displacement (or velocity) field of the model surface at high spatial and temporal resolution (e.g. Adam et al., 2005), which allows further quantification of strain. From the surface deformation we derive a calculated flow field in the silicone layer. Flow field analysis involves Poiseuille and Couette type flow mechanisms. More specifically, it takes into account the pressure gradient in the viscous layer due to differential loading, which results in a Poiseuille channel flow (Warsitzka et al., 2018), while the lateral movement of the overburden induces shear stresses driving Couette shear flow in the viscous layer (see Text S2 and Figure S2 for details). After the experiment, the models are wetted, sequentially sliced, and photographed to provide cross-sectional views.

3 Experimental observations

3.1 Model 1: Progradation With Critical Depositional Slope

In Model 1 (5° critical slope), the sand cover wedge immediately triggers extension (Fig. 2a) occupying ∼10% of the basin length (% b.l.) and contraction affecting ~20 % b.l. with a translational domain of ∼20 % b.l. in between (Figs 2b & 3a). The extensional domain is characterised by two grabens (G1 and G2) while the contractional domain is composed of numerous small-wavelength (1–2 cm) folds and thrusts (F1) (Figs 2b & 3a). After 24 hours, as the sand wedge progrades basinward, an additional graben G3 occurs at 5 cm offset from G2, and an additional fold set (F2) nucleates 5 cm away from F1 (Fig 3a). Simultaneously, the translational domain (TD) increases to ∼30 % b.l. as a part of the contractional domain gets buried and becomes deactivated (Fig. 3a). The translational domain continues to expand reaching >50 % b.l. by the end of the experiment (Fig. 2b). As the translational domain expands, the extensional domain increases to >20 % b.l. until G1 deactivates after 72 hours (Fig. 3a). In contrast, the contractional domain decreases to ∼10 % b.l. after 64 hours until a new fold and thrust set F3 nucleates 10 cm offset from F2 (Fig. 3a). Contemporaneously with the occurrence of F3, a distal contractional structure F5 localizes (Fig. 3a). A final migration of the contraction occurs at 84 hours as the fold and thrust set F4 develops c. 8 cm next to F3 (Fig. 3a).

3.2 Model 1: Progradation With Unstable Depositional Slope

In Model 2 (27° unstable slope), the sand wedge initiates three extensional grabens (G1–G3) and a small-wavelength fold and thrust set (F1) covering ∼10 % b.l. and ∼15 % b.l., respectively, with a translational domain (TD1) in between occupying <5 % b.l. (Fig. 3b). In contrast to Model 1, no deformation occurs in the most landward area as spreading is localized at the wedge front (Figs 3a & b). After 24 hours, a new extensional graben occurs between the initial translational domain (TD1) and the contractional domain, increasing the extensional domain to ∼15 % b.l. (Fig. 3b). Another fold and thrust set F2 forms in the basinward side of F1, followed by F3–F5 between 24–36 hours, increasing the contractional domain to ∼40 % b.l. (Fig. 3b).

During the basinward migration of both domains, the early translational domain (TD1) is overprinted by the extensional domain, while the fold and thrust set (F1) becomes part of the new translational domain (TD2) (Fig. 3b). At 36 hours, contractional structures (F7) localize in the basinward basin edge (Fig. 3b). Around the 60-hour mark, an extensional graben (G5) occurs at the location of F2 while a distal contractional structure F6 also emerges (Fig. 3b). As a result of such markedly synchronous migration of the extensional and contractional domains, the translational domain (TD3) shifts again to the area between F3 and F4 (Fig. 3b). In the landward area, the extensional structures G1–G4 gradually deactivate and only G5 remains active at the end of the experiment (Fig. 3b). A final shift of the translational domain occurs at around 108 hours as F4 starts to extend and the area between F4 and F5 becomes part of the translational domain (TD4) (Fig. 3b). Throughout the experiment, the successive, short lived translational domains of Model 2 occupy a relatively small and constant area (<5 % b.l.), compared to the long lived, expanding translational domain in Model 1 (>50 % b.l.).

4 Discussion

4.1 Wedge dynamics

Our experiments highlight how the spreading dynamics of critical vs. unstable progradational wedges control the structural style and kinematic evolution of gravity-driven deformation in salt basins. The main controversy regarding the role of gravity-spreading in salt tectonics is rooted in the question of whether it is alone a sufficient driver for thin-skinned deformation (e.g. Brun & Fort, 2011; Rowan et al., 2012). Consequently, identifying gravity spreading in nature becomes a key issue in the debate (e.g. Brun & Fort, 2011; Rowan et al., 2012). One of the main diagnostic features of gravity spreading is the development of late extension over early contraction, as both domains migrate basinward along with the progradational wedge (e.g. Brun & Fort, 2011; McClay et al., 1998; Vendeville, 2005). Our Model 2, with a steep, unstable depositional slope exemplifies such archetypical synchronicity (Fig. 3b). In contrast, with a gentle depositional slope, the gravity spreading system in Model 1 is more decoupled and characterized by long lived, expanding extensional and translational domains and a migrating contractional domain.

The kinematic evolution of Model 1 is notably similar to gravity-gliding systems driven by progressive margin tilting (Ge et al., 2019b; their fig. 4). However, flow field analysis shows that the flow mechanism is different from gravity-gliding controlled ones. In both our models, the viscous flow is dominated by Poiseuille flow (Fig. 4a). In contrast, classical gravity-gliding systems are generally dominated by Couette flow (Brun & Fort, 2011). Cross sectional views of the flow field reveal that the viscous flow is widely distributed in Model 1 while localized under the frontal slope in Model 2 (Fig. 4b). Furthermore, the flow velocity in Model 2 is significantly higher resulting in a faster evacuation of the silicone beneath the frontal slope. Consequently, the overburden wedge welds quickly on the base of the silicone locking upslope parts of the wedge and forcing the extensional and contractional domains to migrate downslope. In contrast, the slow expulsion of silicone in Model 1 causes long-lasting deformation throughout the wedge and a relatively slow basinward migration of the extensional domain (Fig. 3a). Consequently, the translational domain expands continuously as the sand wedge propagates, resulting in a basin-wide deformation system (Fig. 3a).

4.2 Comparison with nature

The two models presented here represent two endmembers of sediment-driven gravity-spreading systems, which can be compared to natural prototypes. The Levant Basin in the eastern Mediterranean show typical features of a low-angle wedge propagating over the Messinian salt layer (Cartwright & Jackson, 2008). The restoration demonstrates that the sedimentary wedge had a front slope between 2.3-2.5° from late Pliocene to present day (Fig. 4c). A relatively long (c. 20 km) translational domain developed between the proximal extension and the distal contraction (Cartwright & Jackson, 2008; their figure 9). Such a structural evolution is resembled by the one observed in our Model 1 (Fig. 4c). However, the Levant margin also went through a mild titling of 0.5°. Thus, the gravity-spreading system might have been slightly overprinted by gravity gliding and the salt flow may also vary through time (Evans & Jackson, 2020).

As a contrasting example, in the northern Santos Basin (Brazil), the strata in the "Albian Gap" (the Cabo Frio Fault) is characterised by basinward migrating extension, with early extensional raft being tens of kilometers away from the late extension (Fig. 4d) (Pichel & Jackson, 2020). Such kinematic evolution is similar to the migration of extension from G4 to G5 in Model 2 (Fig. 3b), suggesting a high frontal slope scenario. Basin physiographic analysis show that the slope of the sedimentary wedges is up to 10° in the Cabo Frio area (Berton & Vesely, 2016), much steeper than the surrounding area where the current slope is generally < 1° (Henriksen et al., 2011).

In most cases, sedimentary progradational systems comprise various depositional slopes and sediment supply varies through space and time (e.g. Carvajal et al., 2009). Consequently, these progradational systems tend to have characteristics of both endmembers during their evolution. Moreover, although the two natural cases presented above show typical features of gravity-spreading, other factors, such as margin tilting, basin geometry, and base-salt relief may still contribute locally or temporarily during their evolution (Dooley et al., 2020; Pichel & Jackson, 2020). Even when dominated by gravity-spreading, spatial and temporal variations other than wedge geometry may also play important roles in controlling the deformation. For example, as the direction of sediment progradation comes obliquely to the (basinward) salt flow direction, the extension and contraction driven by sediment wedge may superimpose on the deformation parallel to the salt flow direction, forming complex salt-related structures (Guerra & Underhill, 2012) or basin-scale transfer zones (Brun & Fort, 2018).

5 Conclusions

We use an analogue modelling approach to provide an assessment of the role of spreading controlled by variably steep progradational wedges in gravity-driven salt tectonic systems. Our experimental results suggest that a spreading system with a gentle frontal slope is characterized by an expanding extensional domain, an increasing translational domain, and basinward migration of the contractional domain complimented with a more evenly distributed salt flow across the basin. Such a basin evolution shares kinematic similarities with gravity-gliding systems that are driven by progressive margin tilting. In contrast, a spreading system with a steep, unstable frontal slope induces migrating extensional and contractional domains with a succession of translational domains resulting in a diagnostic structural pattern. The salt flow is more localized beneath the frontal slope of the wedge resulting rapid salt welding and locking of the upslope parts of the wedge. In both cases, salt flow is dominated by Poiseuille flow with only a subordinate contribution from Couette flow thus in contrast to classical gravity-gliding systems dominated by Couette flow. The two models presented in this study are endmembers of gravity-spreading systems. Natural cases may show hybrid characters depending on the wedge stability. Other factors, such as margin tilting, salt thickness and base-salt relief may further complicate the deformation. Our study has important implications in interpreting thin-skinned salt tectonic deformation, such as the Albian Gap in the Santos Basin.

Acknowledgments

ZG thanks the Science Foundation of China University of Petroleum, Beijing (No. 2462020QNXZ002) and L. Meltzers Høyskolefond for financial support. Frank Neumann and Thomas Ziegenhagen are thanked for technical assistance. We thank Nadaya Cubas for providing the script of the critical taper model calculations. We thank Jonathan Bedford for reading an early draft of this paper. GFZ Data Services are thanked for making the data openly accessible. Experimental data of this study will be published open access in Ge et al. (2020).

References

Adam, J., Ge, Z., & Sanchez, M. (2012). Post-rift salt tectonic evolution and key control factors of the Jequitinhonha deepwater fold belt, central Brazil passive margin: Insights from scaled physical experiments. *Marine and Petroleum Geology, 37*(1), 70–100. https://doi.org/10.1016/j.marpetgeo.2012.06.008

Adam, J., & Krezsek, C. (2012). Basin-scale salt tectonic processes of the Laurentian Basin, Eastern Canada: insights from integrated regional 2D seismic interpretation and 4D physical experiments. *Geological Society, London, Special Publications, 363*(1), 331–360. https://doi.org/10.1144/SP363.15

Adam, J., Urai, J. L., Wieneke, B., Oncken, O., Pfeiffer, K., Kukowski, N., et al. (2005). Shear localisation and strain distribution during tectonic faulting—new insights from granular-flow experiments and high-resolution optical image correlation techniques.

Journal of Structural Geology, 27(2), 283–301. https://doi.org/10.1016/j.jsg.2004.08.008

Berton, F., & Vesely, F. F. (2016). Seismic expression of depositional elements associated with a strongly progradational shelf margin: northern Santos Basin, southeastern Brazil. *Brazilian Journal of Geology, 46(4)*, 585-603. https://doi.org/10.1016/j.marpetgeo.2011.03.004

Brun, J.-P., & Fort, X. (2011). Salt tectonics at passive margins: Geology versus models. *Marine and Petroleum Geology, 28*(6), 1123–1145. http://dx.doi.org/10.1590/2317-4889201620160031

Brun, J.-P., & Fort, X. (2018). Growth of Continental Shelves at Salt Margins. *Frontiers in Earth Science, 6*, 1-13. https://doi.org/10.3389/feart.2018.00209

Cartwright, J. A., & Jackson, M. P. A. (2008). Initiation of gravitational collapse of an evaporite basin margin: The Messinian saline giant, Levant Basin, eastern Mediterranean. *Geological Society of America Bulletin, 120*(3-4), 399-413. https://doi.org/10.1130/B26081X.1

Carvajal, C., Steel, R., & Petter, A. (2009). Sediment supply: The main driver of shelf-margin growth. *Earth-Science Reviews, 96*(4), 221-248. https://doi.org/10.1016/j.earscirev.2009.06.008

Cohen, H. A., & Hardy, S. (1996). Numerical modelling of stratal architectures resulting from differential loading of a mobile substrate. In G. I. Alsop, D. J. Blundell, & I. Davison (Eds.), *Salt Tectonics* (Vol. 100, pp. 265–273): Geological Society, London, Special Publications.

Dahlen, F. (1990). Critical taper model of fold-and-thrust belts and accretionary wedges. *Annual Review of Earth and Planetary Sciences, 18*(1), 55-99. https://doi.org/10.1146/annurev.ea.18.050190.000415

Davis, D. M., & Engelder, T. (1985). The role of salt in fold-and-thrust belts. *Tectonophysics, 119*(1), 67-88. https://doi.org/10.1016/0040-1951(85)90033-2

Dooley, T. P., Hudec, M. R., Pichel, L. M., & Jackson, M. P. A. (2020). The impact of base-salt relief on salt flow and suprasalt deformation patterns at the autochthonous, paraautochthonous and allochthonous level: insights from physical models. *Geological Society, London, Special Publications, 476*. https://doi.org/10.1144/SP476.13

Evans, S., & Jackson, C. A.-L. (2020). Intrasalt Structure and Strain Partitioning in Layered Evaporites: Implications for Drilling Through Messinian Salt in the Eastern Mediterranean. *Preprint*.

Fort, X., Brun, J.-P., & Chauvel, F. (2004). Salt tectonics on the Angolan margin, synsedimentary deformation processes. *AAPG Bulletin, 88*(11), 1523–1544. https://doi.org/10.1306/06010403012

Ge, H., Jackson, M. P. A., & Vendeville, B. C. (1997). Kinematics and dynamics of salt tectonics driven by progradation. *AAPG Bulletin, 81*(3), 398–423. https://doi.org/10.1306/522B4361-1727-11D7-8645000102C1865D

Ge, Z., Rosenau, M., & Warsitzka, M. (2020). *Digital image correlation data from analogue modeling experiments addressing the role of spreading in gravity-driven salt tectonics.*

Ge, Z., Rosenau, M., Warsitzka, M., & Gawthorpe, R. L. (2019a). Overprinting translational domains in passive margin salt basins: insights from analogue modelling. *Solid Earth, 10*(4), 1283-1300. https://doi.org/10.5194/se-10-1283-2019

Ge, Z., Warsitzka, M., Rosenau, M., & Gawthorpe, R. L. (2019b). Progressive tilting of salt-bearing continental margins controls thin-skinned deformation. *Geology, 47*(12), 1122-1126. https://doi.org/10.1130/G46485.1

Gemmer, L., Beaumont, C., & Ings, S. J. (2005). Dynamic modelling of passive margin salt tectonics: effects of water loading, sediment properties and sedimentation patterns. *Basin Research, 17*(3), 383–402. https://doi.org/10.1111/j.1365-2117.2005.00274.x

Gradmann, S., Beaumont, C., & Albertz, M. (2009). Factors controlling the evolution of the Perdido Fold Belt, northwestern Gulf of Mexico, determined from numerical models. *Tectonics, 28*(2). https://doi.org/10.1029/2008TC002326

Guerra, M. C. M., & Underhill, J. R. (2012). Role of halokinesis in controlling structural styles and sediment dispersal in the Santos Basin, offshore Brazil. *Geological Society, London, Special Publications, 363*(1), 175-206. https://doi.org/10.1144/SP363.9

Henriksen, S., Helland-Hansen, W., & Bullimore, S. (2011). Relationships between shelf-edge trajectories and sediment dispersal along depositional dip and strike: a different approach to sequence stratigraphy. *Basin Research, 23*(1), 3-21. https://doi.org/10.1111/j.1365-2117.2010.00463.x

Krézsek, C., Adam, J., & Grujic, D. (2007). Mechanics of fault and expulsion rollover systems developed on passive margins detached on salt: insights from analogue modelling and optical strain monitoring. *Geological Society, London, Special Publications, 292*(1), 103–121. http://dx.doi.org/10.1144/SP292.6

Lugo-Fernández, A., & Morin, M. M. (2004). Slope and Roughness Statistics of the Northern Gulf of Mexico Seafloor With Some Oceanographic Implications. *Gulf of Mexico Science, 22*(1). https://doi.org/10.18785/goms.2201.03

McClay, K. R., Dooley, T., & Lewis, G. (1998). Analog modeling of progradational delta systems. *Geology, 26*(9), 771–774. https://doi.org/10.1130/0091-7613(1998)026<0771:AMOPDS>2.3.CO;2

Nemec, W. (1990). Aspects of Sediment Movement on Steep Delta Slopes. In A. Colella & D. Prior (Eds.), *Coarse-Grained Deltas* (pp. 29-73): International Assocication of Sedimentologist Special Publication.

Patruno, S., & Helland-Hansen, W. (2018). Clinoforms and clinoform systems: Review and dynamic classification scheme for shorelines, subaqueous deltas, shelf edges and continental margins. *Earth-Science Reviews, 185*, 202-233. https://doi.org/10.1016/j.earscirev.2018.05.016

Pichel, L. M., & Jackson, C. A. (2020). The Enigma of the Albian Gap: Spatial Variability and the Competition Between Salt Expulsion and Extension. *Journal of the Geological Society*. https://doi.org/10.1144/jgs2020-055

Prather, B. E., O'Byrne, C., Pirmez, C., & Sylvester, Z. (2017). Sediment partitioning, continental slopes and base-of-slope systems. *Basin Research, 29*(3), 394-416. https://doi.org/10.1111/bre.12190

Raillard, S., Vendeville, B. C., & Gue´rin, G. (1997). *Causes and structural characteristics of thin-skinned inversion during gravity gliding or spreading above salt or shale*. Paper presented at the AAPG Annual Convention Official Program. http://www.searchanddiscovery.com/abstracts/html/1997/annual/abstracts/0095d.htm

Roberts, H., McBride, R., & Coleman, J. (1999). Outer shelf and slope geology of the Gulf of Mexico: an overview. *The Gulf of Mexico Large Marine Ecosystem: Blackwell Science*.

Ross, W., Halliwell, B., May, J., Watts, D., & Syvitski, J. (1994). Slope readjustment: a new model for the development of submarine fans and aprons. *Geology, 22*(6), 511-514. https://doi.org/10.1130/0091-7613(1994)022<0511:SRANMF>2.3.CO;2

Rowan, M. G., Peel, F. J., & Vendeville, B. C. (2004). Gravity-driven fold belts on passive margins. In K. R. McClay (Ed.), *Thrust tectonics and hydrocarbon systems* (pp. 157–182): AAPG Memoir.

Rowan, M. G., Peel, F. J., Vendeville, B. C., & Gaullier, V. (2012). Salt tectonics at passive margins: Geology versus models–Discussion. *Marine and Petroleum Geology, 37*(1), 184-194. https://doi.org/10.1016/j.marpetgeo.2012.04.007

Schlager, W., & Camber, O. (1986). Submarine slope angles, drowning unconformities, and self-erosion of limestone escarpments. *Geology, 14*(9), 762-765. https://doi.org/10.1130/0091-7613(1986)14<762:SSADUA>2.0.CO;2

Vendeville, B. C. (2005). Salt tectonics driven by sediment progradation: Part I—Mechanics and kinematics. *AAPG Bulletin, 89*(8), 1071–1079. https://doi.org/10.1306/03310503063

Warsitzka, M., Kukowski, N., & Kley, J. (2018). Salt flow direction and velocity during subsalt normal faulting and syn-kinematic sedimentation—implications from analytical calculations. *Geophysical Journal International, 213*(1), 115-134. https://doi.org/10.1093/gji/ggx552

Figure caption

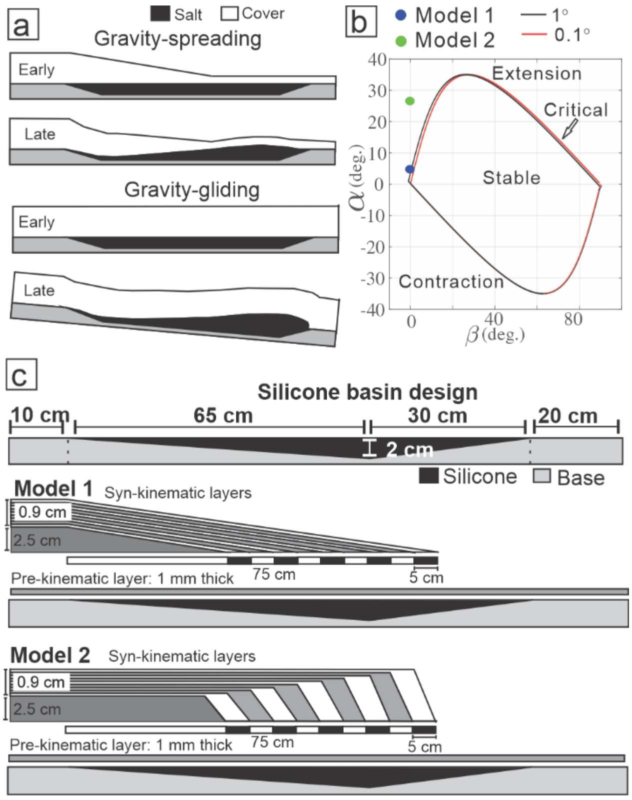

Figure 1. (a) Gravity-gliding vs. gravity-spreading systems (modified after Allen et al., 2016). (b) Wedge stability analysis using Critical Wedge Theory (CWT). The two wedge geometries are plotted together with the CWT predicted stability fields (see Text S1 and Figure S1 for details). The two curves correspond to viscous strength equivalent basal friction angles of 0.1° and 1° representing the expected range of basal strength. (c) Cross-sectional view of the model design. Note the different geometries of two progradational wedges.

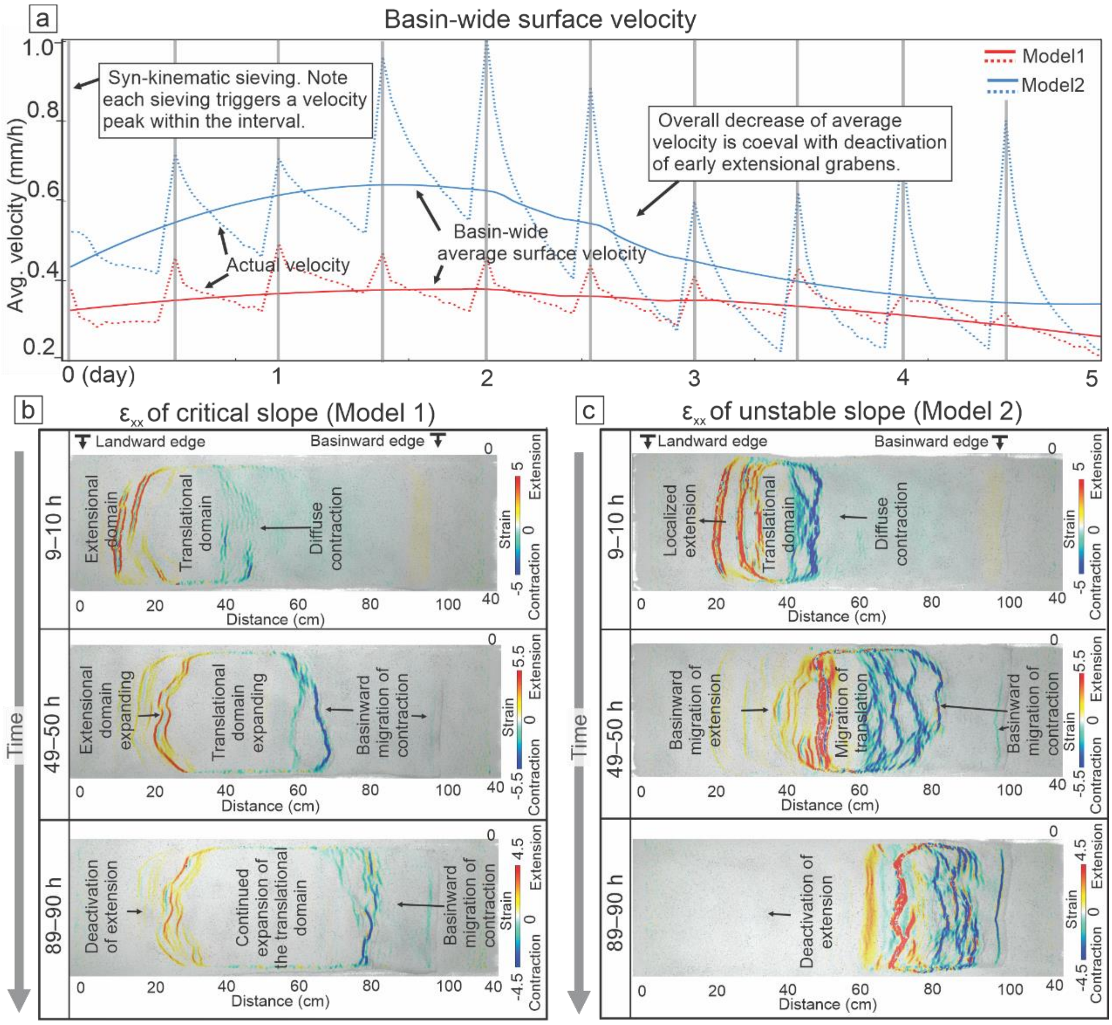

Figure 2. (a) Surface velocity vs. time for models 1 and 2. Note the higher rates in Model 2 relative to Model 1. Input of sediment triggers transient increase in velocity. (b–c) Map views of incremental longitudinal surface strain (ε_{xx}) in Model 1 (b) and 2 (c) at early (9–10 h), mid (49–50 h) and late (89–90 h) stages during the experiment.

442
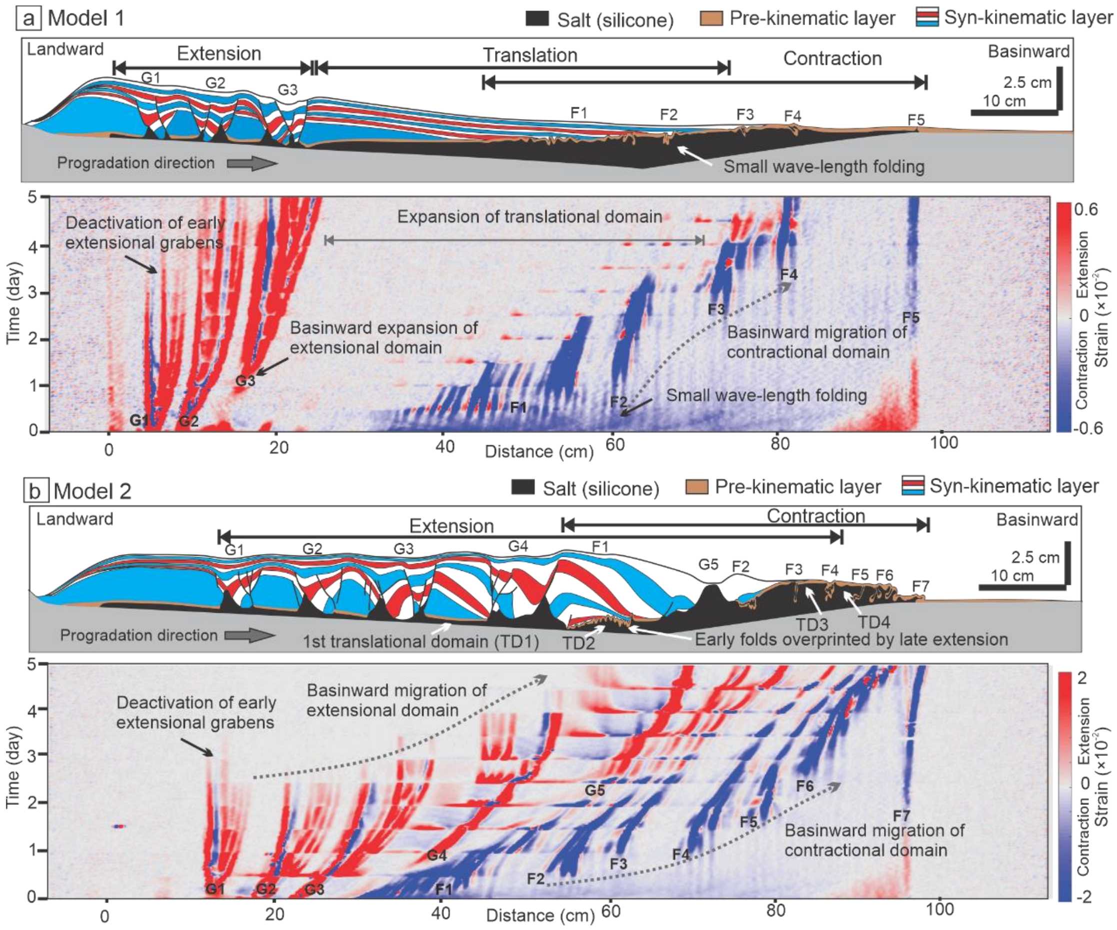

443 **Figure 3**. (a) Cross sections and longitudinal surface strain rate map of Model 1. Note
444 the expansion of extensional and translational domains as well as the basinward
445 migration of the contractional domain. (b) Cross section and longitudinal surface
446 strain rate map of Model 2. Note the synchronized basinward migration of both
447 extension and contraction and the shifts of the translational domain (TD). Strain rate
448 maps are constructed by plotting strain rate (1 h increments) along a central profile (x
449 axis) over time (y axis).
450

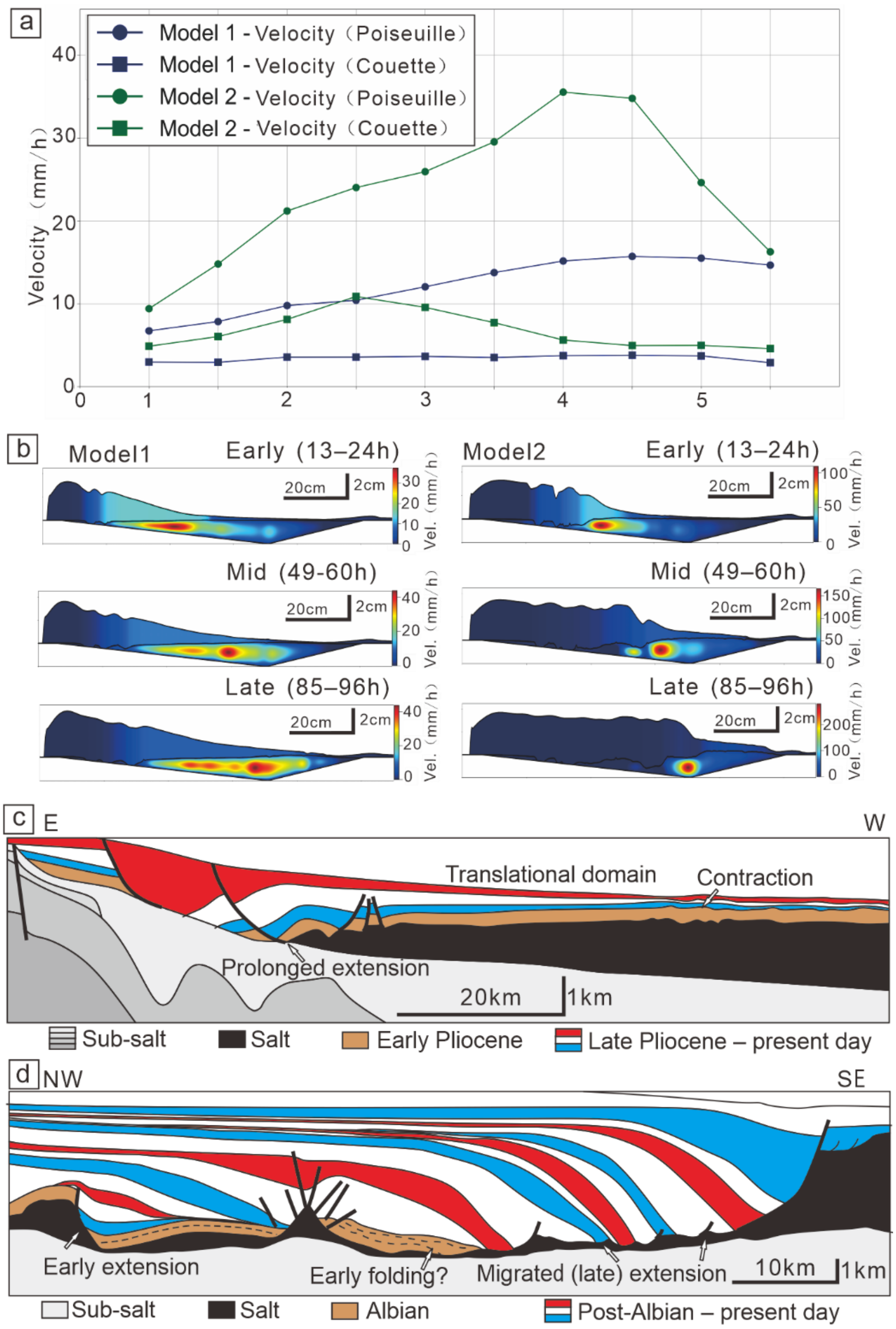

Figure 4. (a) Silicone flow analysis based on velocity profile (Text S2 and Figure S2). In both models, Poiseuille flow dominates over Couette flow. (b) Representative velocity profiles from early (13–24 h), mid (49–60h) and late (85–96h) stages during model evolution. Note the more evenly distributed viscous flow in Model 1 and more localized viscous flow in Model 2. (c) Cross section along the Levant margin in the eastern Mediterranean. Note the translational domain in the mid slope and its overall similarity to Model 1 (modified from Fig. 9 in Cartwright & Jackson, 2008). (d) South-central section of the Albian Gap (the Cabo Frio Fault). Note the early and late (migrated) extension and possible early contraction underneath (modified from Fig. 7 in Pichel & Jackson, 2020).